Bandwidth-reduced Brillouin optical time-domain analysis based on a quarter of the frequency of modulation

ZHANG Xiangfei[1,2], WEI Zhengjun[1,2]*, ZHENG Yingfang[1,2], and WANG Jindong[1]

1. *Guangdong Provincial Key Laboratory of Quantum Engineering and Quantum Materials, South China Normal University, Guangzhou 510006, China*

2. *Guangdong Provincial Key Laboratory of Nanophotonic Functional and Devices, South China Normal University, Guangzhou 510006, China*

Aiming at the problem of high requirement for the signal generator in the Brillouin optical time-domain analysis (BOTDA) system, a quarter of the Brillouin frequency shift (BFS) of modulation is proposed to reduce the required bandwidth of the sensing system. A functional model for solving the intensity of each-order sideband of the output light of electro-optic modulator (EOM) is proposed and applied, so the spectrum with suppressed the carrier and the first-order sidebands while maximizing the second-order sidebands is obtained. Compared with the latest scheme, the intensity of the second-order sidebands is increased by 21.1% based on this functional model. In the experiment, the second-order upper sideband and the second-order lower sideband are used as continuous wave (CW) probe light and pump pulse light, respectively, which ultimately reduces the required bandwidth of radio frequency (RF) signal sources to a quarter of the BFS (reduced from ~11 GHz to ~2.75 GHz), and the frequency sweep range is also reduced to a quarter of the original.

Distributed optical fiber sensing system based on Brillouin scattering has been extensively researched in the past few decades due to its capabilities of measuring temperature and strain over the sensing fibers[1-5]. The scheme of Brillouin optical time-domain analysis (BOTDA) is much preferred due to its high spatial resolution, long measuring distance, and simultaneous measurement of temperature and strain[6]. BOTDA uses the stimulated Brillouin scattering (SBS) effect to inject two counter-propagating light beams from both ends of the fiber[7], i.e., a pump pulse and a continuous wave (CW) probe wave. By sweeping the probe light, the frequency difference between the pump light and the probe light is changed, and the Brillouin gain spectrum (BGS) along the optical fiber is reconstructed. Moreover, the Brillouin frequency shift (BFS) is obtained by Lorentz fitting or other methods for BGS, and the temperature and strain are obtained after demodulation[8].

In a fast BOTDA (F-BOTDA) system, frequency-agility radio frequency (RF) signal needs to be applied on an electro-optic modulator (EOM) to obtain the first-order upper or lower sideband of the modulated light[9]. A conventional modulation scheme usually employs an arbitrary waveform generator (AWG) to generate such a signal. Unfortunately, as described by PELED et al[10], it is very difficult to find an available commercial AWG to output RF signal with adjustable frequency at ~11 GHz (the BFS in ordinary silica fiber), which often requires complex modulation methods.

To this end, DONG et al[11] proposed the scheme of second-order sideband of modulation in 2013, which used the second-order sideband as the probe light through appropriately adjusting the operating point of the modulator with the carrier and odd-order sidebands of the modulated light being suppressed, and subsequently reducing the bandwidth requirements of the AWG by half to ~5.5 GHz. Since this method, a lot of works have explored the prospect of the second-order sideband of modulation. In 2016, BA et al[12] utilized the second-order sideband modulation scheme based on multi-slope assisted F-BOTDA, which reduced the required bandwidth by half and realized faster measurement. In 2018, DONG et al[13] proposed that the second-order sideband of modulation can be used in the BOTDA system based on frequency agility technology, and afterward, they demonstrated the feasibility of the second-order sideband of modulation in ultra-fast distributed Brillouin optical fiber sensing for dynamic strain measurement in 2019[14]. Although the second-order sideband of modulation reduces the bandwidth requirement of the AWG by half, the intensity of useful second-order sideband is not maximized, and the required

---

bandwidth of system is still too high, which is still not conducive to the popularization and marketization of BOTDA.

In this paper, we analyze the light frequency shift characteristics of EOM and propose a functional model for solving the intensity of each-order sideband of the modulated light. Compared with the traditional second-order sideband of modulation scheme, the useful signal obtained based on the proposed function model reaches the maximum value, and its intensity is increased by 21.1%. We propose an improved BOTDA system based on a quarter of the frequency of modulation, which pre-modulates the incident light and extracts the second-order upper sideband and lower sideband as pulsed light and probe light, respectively. In comparison with traditional system structure, the bandwidth requirement of BOTDA system is reduced to a quarter of the original (reduce from ~11 GHz to ~2.75 GHz).

Provided that the voltage acting on the EOM in Mach-Zehnder interferometer (MZI) configuration is $V=V_{DC}+V_{RF}\cos(w_{RF}t)$, where V_{DC} is the direct current (DC) bias voltage, V_{RF} is the RF modulation voltage, and w_{RF} is the angular frequency of the RF modulation voltage, and then the modulated light[15] can be expressed as

$$E(t) = E_0 \exp\left(jw_0 t \right)\cos\left[C \cdot \cos\left(w_{RF}t \right) + \varphi_{DC} \right], \quad (1)$$

where E_0 is the amplitude of the input optical field, w_0 is the angular frequency of the incident light, $C=\pi V_{RF}/(2V_\pi)$ is the modulation depth, V_π is the half-wave voltage, and $\varphi_{DC}=\pi V_{DC}/(2V_\pi)$ is the phase caused by the DC bias voltage. Eq.(1) can also be expressed as

$$E(t) = E_0 \cos(w_0 t)\{[J_0(C) +$$
$$2\sum_{n=1}^{\infty} J_{2n}(C) \times \cos(2nw_{RF}t)]\cos\varphi_{DC} -$$
$$[2\sum_{n=0}^{\infty}(-1)^n J_{2n+1}(C) \cdot \cos(2n+1)w_{RF}t]\sin\varphi_{DC}\}, (2)$$

where $J_n(x)$ is Bessel function of the first kind.

To quantitatively analyze the influence of different parameters on the intensity of each-order sideband of modulated light, I_n is used to express the intensity of the n-th order sideband in the EOM output light, and I_n can be written as

$$I_n = \frac{1}{2} E_0^2 J_n^2(C)\left[1 + (-1)^n \cos(2\varphi_{DC})\right], n \in Z. \quad (3)$$

In the experiment, the incident light is usually kept unchanged, so the light intensity of the n-th order sideband can be changed by adjusting the amplitudes of V_{RF} and V_{DC}. Accordingly, we propose a functional model $I_n(V_{RF}, V_{DC})$ with two variables (V_{RF} and V_{DC}) to describe the intensity of the n-th order sideband in the output light, shown as

$$I_n(V_{RF}, V_{DC}) = \frac{1}{2} E_0^2 J_n^2\left(\pi \frac{V_{RF}}{2V_\pi} \right)[1+$$
$$(-1)^n \cos\left(\pi \frac{V_{DC}}{V_\pi} \right)], n \in Z, \quad (4)$$

where J_n will decrease as n increases, so we only need to pay attention to the intensities of the carrier ($n=0$), first-order sideband ($n=1$) and second-order sideband ($n=2$) in BOTDA, shown as
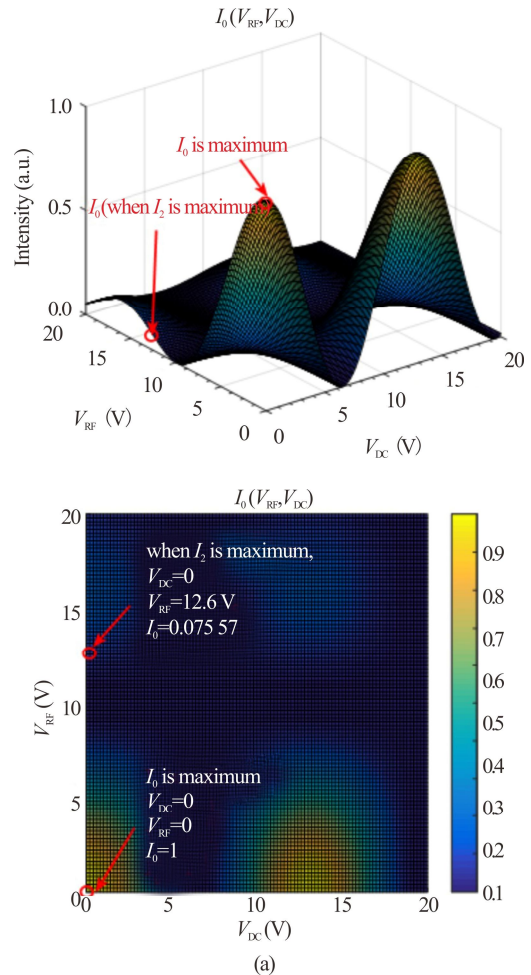
$$I_0(V_{RF}, V_{DC}) = \frac{1}{2} E_0^2 J_0^2\left(\pi \frac{V_{RF}}{2V_\pi} \right)\left[1 + \cos(\pi \frac{V_{DC}}{V_\pi})\right], \quad (5)$$

$$I_1(V_{RF}, V_{DC}) = \frac{1}{2} E_0^2 J_1^2\left(\pi \frac{V_{RF}}{2V_\pi} \right)\left[1 - \cos(\pi \frac{V_{DC}}{V_\pi})\right], \quad (6)$$

$$I_2(V_{RF}, V_{DC}) = \frac{1}{2} E_0^2 J_2^2\left(\pi \frac{V_{RF}}{2V_\pi} \right)\left[1 + \cos(\pi \frac{V_{DC}}{V_\pi})\right]. \quad (7)$$

Under the assumption that the value of V_π is 6.5 V, we draw a three-dimensional graph to show the intensity of the n-th ($n=0$, 1 and 2) order sidebands with V_{RF} and V_{DC}, as shown in Fig.1.

According to the functional model $I_n(V_{RF}, V_{DC})$, we set $V_{DC}=0$, $V_{RF}=12.6$ V ($C=3.1$), which makes the intensity of the second-order sidebands reach the maximum value of 0.237, the intensity of the zero-order sideband is 0.076, and the first-order sidebands vanish. In the case of $C=3.1$, the output spectra of the modulator are shown in Fig.2, which shows that the carrier is effectively suppressed, the first-order sidebands are completely suppressed, and the second-order sidebands are maximized.
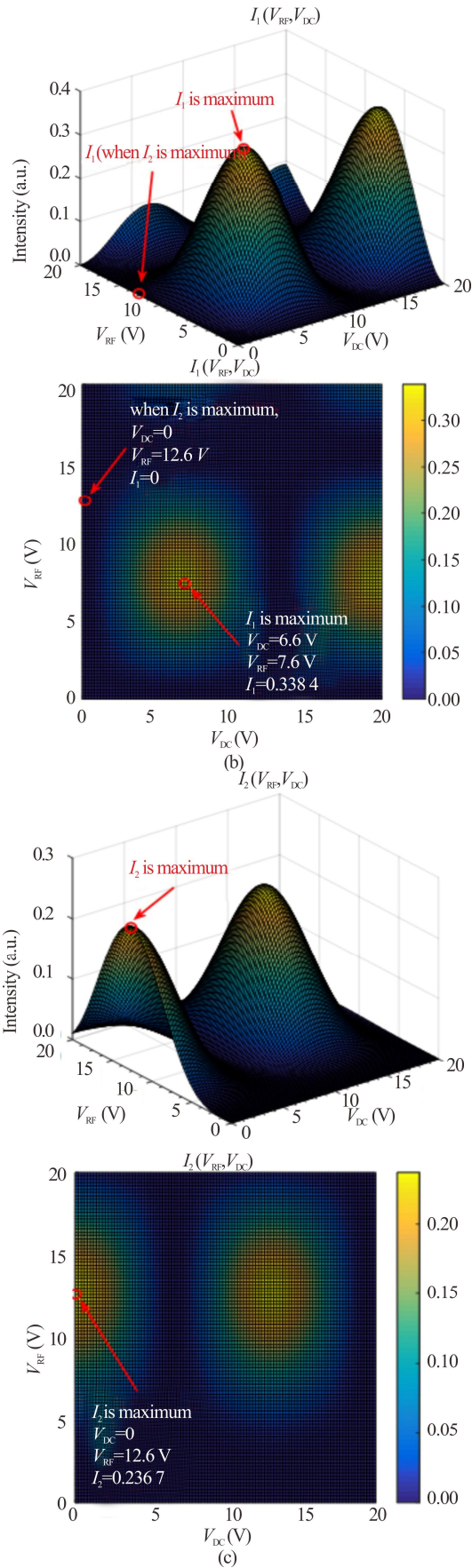

(a)

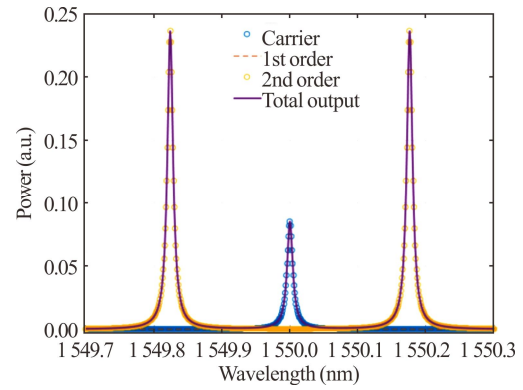Fig.1 Intensity of the *n*-th sideband: (a) *n*=0; (b) *n*=1; (c) *n*=2

Fig.2 Output spectra realized by the proposed function model $I_n(V_{RF}, V_{DC})$

The principle of traditional second-order sideband of modulation is as follows. Let the DC bias voltage operate at the maximum point of transmission characteristic curve of the EOM, so that the first-order sidebands vanish. Since the zero-points of the Bessel functions corresponding to different-order sidebands are different, adjust V_{RF} to make $J_0(C)|_{C=2.405}=0$, so that the zero-order sideband (carrier) vanishes. The carrier and first-order sidebands in the output light are completely suppressed, and only the useful second-order sidebands are retained at last. Under this condition, the output of the modulator is shown in Fig.3.
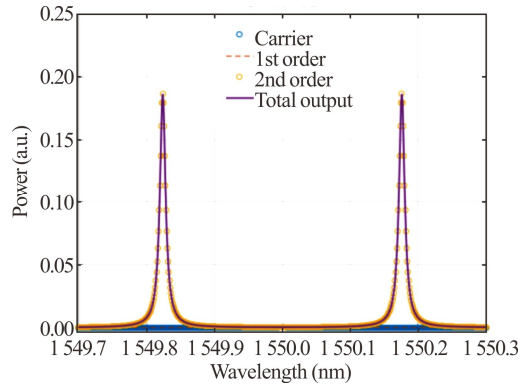

Fig.3 Output spectra realized by the traditional second-order sideband of modulation

Purer second-order sidebands are achieved by the second-order sideband of modulation, but the intensity is only 78.9% of the maximum value. Fortunately, according to the functional model $I_n(V_{RF}, V_{DC})$ proposed in this paper, setting the appropriate parameters of the modulator can obtain the maximized second-order sidebands. As for the residual low-intensity carrier, it can be filtered out by a bandpass optical filter with a 3 dB bandwidth of 11 GHz or less.

In summary, this paper uses the functional model $I_n(V_{RF}, V_{DC})$ to quantitatively analyze the intensity of each-order sideband in the modulated light, and optimizes the second-order sideband of modulation, which
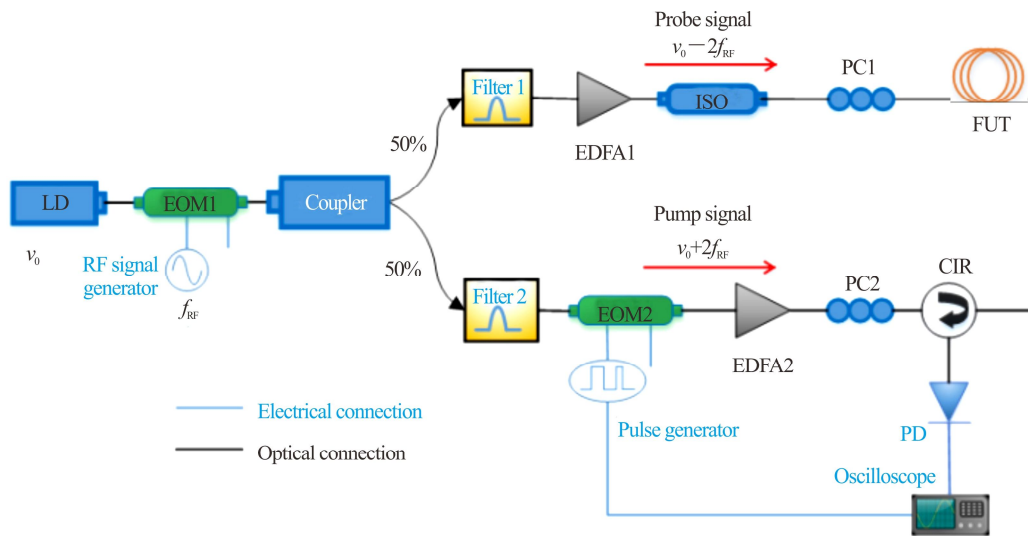
can maximize the useful signal in the BOTDA system. What's more, the model is also applicable to most EOM-based optical fiber communication and sensing systems, which demonstrates that the functional model has good practicability and expansibility.

In a conventional BOTDA system, to make the frequency difference of the two light beams close to the BFS of v_B (~11 GHz), the frequency of RF modulating signal on EOM needs to satisfy $f_{RF} \approx v_B$[16], while the second-order sideband of modulation[11] is proposed to choose the second-order upper or lower sideband from the modulated light as the probe wave, which can reduce f_{RF} by half, i.e., $f_{RF} \approx \frac{1}{2}v_B$. In this paper, the second-order sideband of modulation is ameliorated based on the function $I_n(V_{RF}, V_{DC})$ and the BOTDA system structure is optimized, so that the required bandwidth of the RF modulated signal is reduced by half, i.e., $f_{RF} \approx \frac{1}{4}v_B$. The structure of the optimized BOTDA system is shown in Fig.4.

The BOTDA system based on a quarter of the BFS of modulation is then experimentally demonstrated. A narrow linewidth (~1 MHz) LD operating at v_0 (about 193.414 489 THz, corresponding to the wavelength of 1 550 nm) is used as the light source, which delivers an output power of 16 dBm. The RF signal source is ADF5355 from Analog Devices, which generates a frequency range of from 54 MHz to 13.6 GHz. Driven by the microcontroller and the RF amplifier, it can meet the experimental requirements. After measurement, the typical V_π of EOM is 6.5 V, and the extinction ratio (*ER*) of EOM is larger than 30 dB, up to 40 dB. By adjusting $V_{DC}=0$ and $V_{RF}=12.6$ V on the EOM1, we make the second-order sidebands dominant and the others suppressed in the output spectrum. A 3 dB optical coupler is employed to split the pre-modulated light from EOM1 into upper and lower branches. Then, the second-order upper sideband (around v_0+2f_{RF}) of the upper branch is extracted through Filter1 with a center wavelength of 1 549.956 nm. Similarly, the second-order lower sideband (around v_0-2f_{RF}) of the lower branch is extracted through Filter2 with a center wavelength of 1 550.044 nm. Both filters are ultra-narrowband bandpass optical filters with a minimum 3 dB bandwidth of 1 GHz. The second-order upper sideband is amplified by EDFA1 and chosen as the probe wave. The CW light from Filter2 can be used as pump wave after being modulated by pulse generator in EOM2 and amplified by EDFA2 to 21.2 dBm. The function/arbitrary waveform generator is DG4162 from Rigol, which is used as pulse generator to output eclectic pulses with a period of 10 μs and a pulse width of 100 ns. PC1 and PC2 are used to ensure that the pump wave and the probe wave are launched on the same main axis of the sensing fiber.

In the experiment, the FUT is an ITU-T G.652.D-compliant optical fiber, Corning SMF-28e, with a total length of ~1 km. The PD converts the optical signal into electrical signal, which is sampled ($f_{sampling}=2$ GHz/s) and stored by an oscilloscope for subsequent processing. Finally, the frequency difference between the probe light and the pump light is $\Delta v=|(v_0-2f_{RF})-(v_0+2f_{RF})|=4f_{RF}$, which meets the requirement of $\Delta v \approx v_B$. In a quarter of the BFS of modulation, the frequency of RF modulation signal is only a quarter of the BFS to drive the electro-optical modulator, which is sufficient to make the frequency difference between the two branch light beams meet the SBS condition[17]. Eventually, a bandwidth-reduced BOTDA based on a quarter of the frequency of modulation is proved effective.

LD: laser device; EOM: electro-optical modulator; Filter: ultra-narrowband bandpass optical filter; EDFA: erbium-doped fiber amplifier; ISO: optical isolator; CIR: circulator; PD: photodetector; FUT: fiber under test; PC: polarization controller

Fig.4 Experimental setup based on a quarter of the frequency of modulation

By adjusting the parameters of the EOM1 properly, the second-order sidebands in the output spectrum are maximized, and the waveforms are shown in Fig.5.
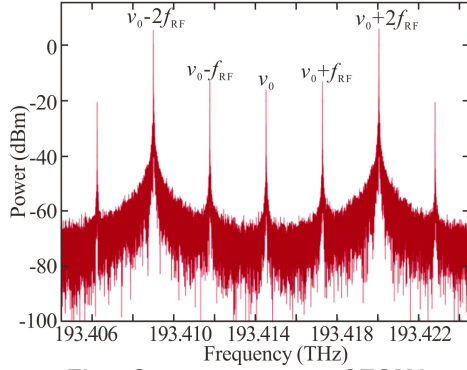

Fig.5 Output spectrum of EOM1

Then, Gaussian narrow-band bandpass optical filters are used to select the optical wave with the frequency of $\sim(v_0-2f_{RF})$ and the frequency of $\sim(v_0+2f_{RF})$ in the output spectrum respectively. In this way, the CW probe light and the pump pulse light with a frequency difference of $4f_{RF}$ are obtained on the two branches, as shown in Fig.6 and Fig.7.

The frequency of the RF signal generator is scanned from 2.725 GHz to 2.775 GHz with a step of 1 MHz and a switching time of 10 ms, so that the frequency difference between probe wave and pump pulses is down-shifted from 10.9 GHz to 11.1 GHz with a step of 4 MHz and the frequency number of N=51. We found that the output frequency range of the RF modulation signal is merely 50 MHz (2.725 GHz to 2.775 GHz) when the range of the frequency difference of the two optical signals is set to 200 MHz (10.9 GHz to 11.1 GHz).

In other words, the scheme of a quarter of the frequency of modulation can not only reduce the required bandwidth of the RF signal source to a quarter of the BFS, but also reduce the output range to a quarter of the original, which undoubtedly reduces the requirement of RF signal source.

The electrical signal converted by the photodetector is stored by the oscilloscope, and then a series of time (space)-intensity curves distributed along the fiber are rearranged by frequency to obtain the distribution of the BGS at each point along with the fiber[18], as shown in Fig.8.
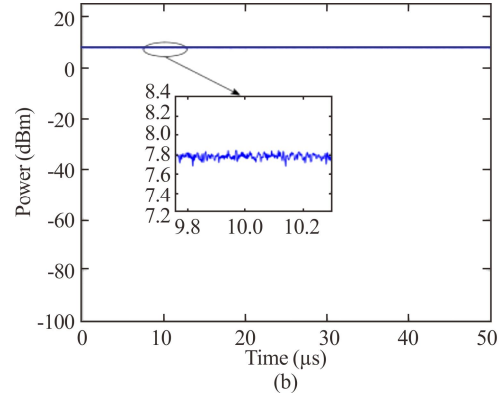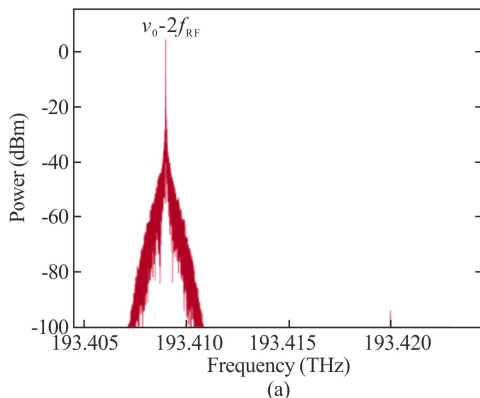

(a)

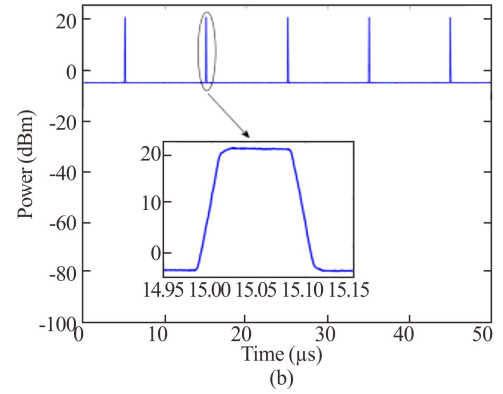**Fig.6 CW probe with a frequency of v_0-2f_{RF}: (a) Spectrum; (b) Wave shape**
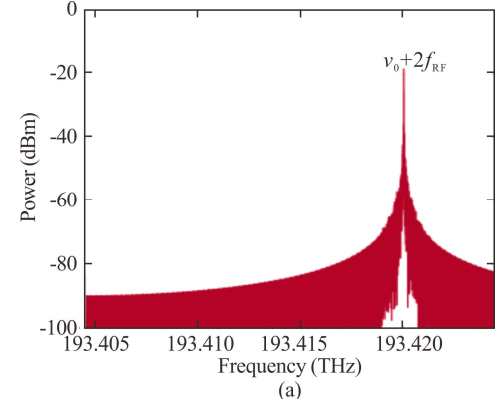

(a)

(b)

Fig.7 Pump pulse with a frequency of v_0+2f_{RF}: (a) Spectrum; (b) Wave shape
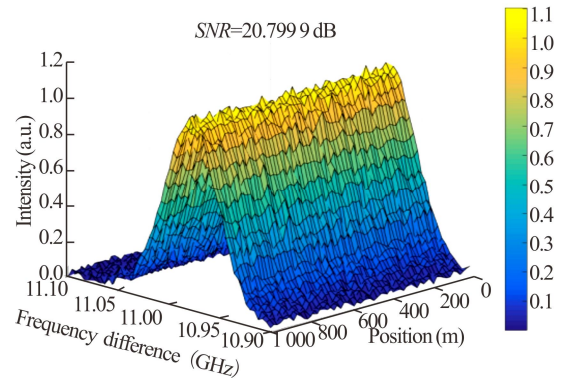

Fig.8 BGS arranged by frequency

As can be seen from the above figure, the BGS distribution diagram not only contains the peak value, frequency

shift, and spectrum width of the BGS along with each point of the fiber, but also contains the noise introduced during the measurement. Before extracting the BFS information at each point on the optical fiber, the actual measured data should be de-noised to preliminarily reduce the impact of noise on the extraction of BFS[19].

In this experiment, the oscilloscope is used to average the sampled backscattered signal 1 000 times, and then wavelet transform is performed on the averaged signal in MATLAB. The de-noising results are shown in Fig.9.
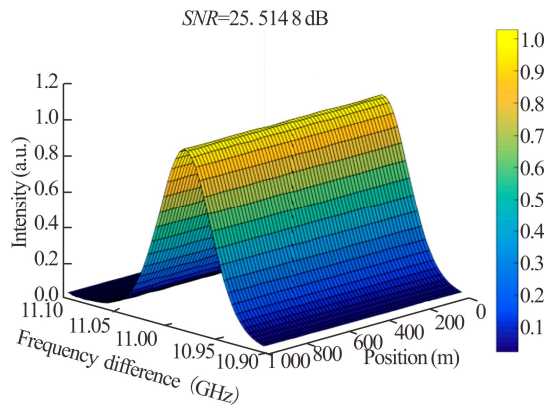

Fig.9 Denoised BGS

Fig.10 Comparison between the ideal BGS and the BGS containing noise: (a) Distribution of $g_r(v)$ and $g_u(v)$; (b) Distribution of $G_m(v)$

After denoising, the signal-to-noise ratio (*SNR*) of the BGS increased from 20.80 dB to 25.51 dB, and the signal waveform is significantly improved, which is convenient for further processing.

To extract BFS quickly and reduce the time of signal processing, the cross-correlation convolution method is used to process the BGS[20]. It is assumed that $g_r(v)$ is an ideal Lorentz-type BGS preset with a central frequency of 10.9 GHz and spectrum width (full width at half maximum, *FWHM*)[21] of 32 MHz, and $g_u(v)$ is the actual BGS containing noise, whose center frequency and spectrum width need to be determined. $G_m(v)$ is the convolution result of ideal BGS with actual noisy BGS, i.e., $G_m(v) = g_r(v) \otimes g_u(v)$. The convolution result of the ideal Lorentz-type BGS curve and the noisy BGS curve is shown in Fig.10.

Fig.10 shows that the shape of the curve after convolution is smoother, and it is directly seen that the center frequency is 21.88 GHz and spectrum width is 90 MHz. Then we calculate that the center frequency is 10.98 GHz and the spectrum width is 58 MHz of the actual BGS. By comparison, the cross-correlation convolution method can not only avoid the high computational complexity caused by the traditional curve fitting method but also ensure good accuracy under the condition of low *SNR*.

In conclusion, we demonstrate a BOTDA system that reduces the bandwidth requirement based on a quarter of the BFS of modulation. A functional model $I_n(V_{RF}, V_{DC})$ for solving the intensity of each-order sideband in the output light of EOM is proposed and applied, which increases the intensity of the useful signal by 21.1%. We o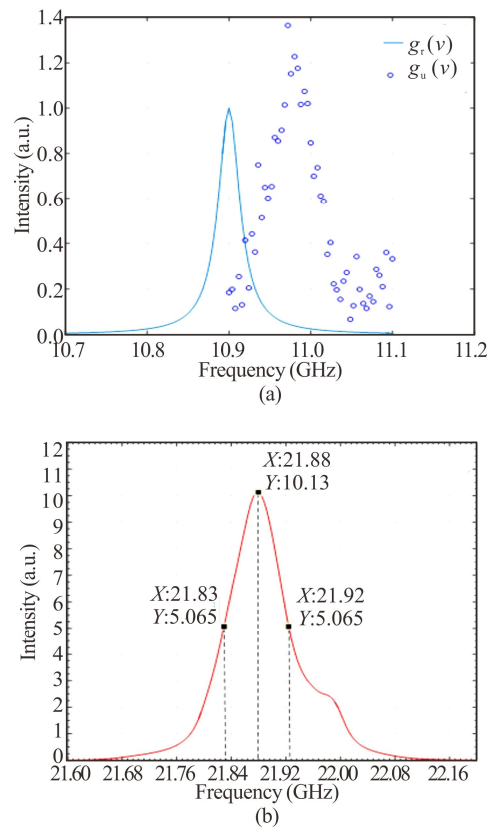ptimize the BOTDA system structure, which reduces the required bandwidth of the RF modulated signal from ~11 GHz to ~2.75 GHz. More practically, the functional model $I_n(V_{RF}, V_{DC})$ can be applied to most EOM-based optical fiber communication and sensing systems, and the improvement of the traditional BOTDA system structure based on a quarter of the frequency of modulation does not require the introduction of additional instruments, which has a high reference value for the popularization and marketization of BOTDA. In addition, the sampled signal processed by the cumulative average and wavelet denoising makes the signal waveform smoother, and improves the *SNR* by 4.71 dB. The cross-correlation convolution method greatly reduces the distortion and high computational complexity caused by the traditional fitting algorithm.

Statements and Declarations

The authors declare that there are no conflicts of interest related to this article.

References

[1]　BAO X Y, CHEN L. Recent progress in distributed fiber optic sensors[J]. Sensors, 2012, 12(12)：8601-8639.

[2]　LIU J Y, WANG T, ZHANG Q, et al. Research progress on temperature-strain dual-parameter sensing in BOTDA system[J]. Laser & optoelectronics progress,

2021, 58(13)：1306021. (in Chinese)

[3]   ZHENG H, YAN Y, WANG Y Y, et al. Deep learning enhanced long-range fast BOTDA for vibration measurement[J]. Journal of lightwave technology, 2022, 40(1)：262-268.

[4]   MOTIL A, BERGMAN A, TUR M. State of the art of Brillouin fiber-optic distributed sensing[J]. Optics & laser technology, 2016, 78：81-103.

[5]   FENG W Q, YIN J H, BORANA L, et al. A network theory for BOTDA measurement of deformations of geotechnical structures and error analysis[J]. Measurement, 2019, 146：618-627.

[6]   ZHU T, ZHENG H, ZHANG J D. Progress in research of Brillouin optical time domain analysis for dynamic strain sensing[J]. Journal of applied sciences, 2012, 38(2)：197-214. (in Chinese)

[7]   SOVRAN I, MOTIL A, TUR M. Frequency-scanning BOTDA with ultimately fast acquisition speed[J]. IEEE photonics technology letters, 2015, 27(13)：1426-1429.

[8]   WANG B W, GUO N, WANG L, et al. Robust and fast temperature extraction for Brillouin optical time-domain analyzer by using denoising autoencoder-based deep neural networks[J]. IEEE sensors journal, 2019, 20(7)：3614-3620.

[9]   SONG M P, ZHAO B, ZHANG X M. Brillouin optical time domain analysis distributed optic-fiber sensor based on microwave electrooptic modulation[J]. Acta optica sinica, 2005, 25(8)：1053-1056.

[10]   PELED Y, MOTIL A, TUR M. Fast Brillouin optical time domain analysis for dynamic sensing[J]. Optics express, 2012, 20(8)：8584-8591.

[11]   DONG Y K, BA D X, JIANG T F, et al. High-spatial-resolution fast BOTDA for dynamic strain measurement based on differential double-pulse and second-order sideband of modulation[J]. IEEE photonics journal, 2013, 5(3)：2600407-2600407.

[12]   BA D X, WANG B Z, ZHOU D W, et al. Distributed measurement of dynamic strain based on multi-slope assisted fast BOTDA[J]. Optics express, 2016, 24(9)：9781-9793.

[13]   DONG Y K, ZHOU D W, WANG B Z. Brillouin optical time-domain analysis at a high sampling rate (invited)[J]. Journal of physics conference, 2018, 1065：252009.

[14]   DONG Y K. Ultra-fast distributed Brillouin optical fiber sensing for dynamic strain measurement[C]//2019 International Photonics and Optoelectronics Meeting (POEM), November 11-14, 2019, Wuhan, China. Washington, DC：Optica Publishing Group, 2019：OFW1A.2.

[15]   ZHOU H J, MENG Z, LIAO Y. Frequency shift characteristics analysis of $LiNbO_3$ waveguide electro-optic intensity modulator[J]. Chinese journal of lasers, 2009, 36(4)：901-905.

[16]   LOPEZ-MERCADO C A, KOROBKO D A, ZOLOTOVSKII I O, et al. Application of dual-frequency self-injection locked DFB laser for Brillouin optical time domain analysis[J]. Sensors, 2021, 21(20)：6859.

[17]   YENIAY A, DELAVAUX J M, TOULOUSE J. Spontaneous and stimulated Brillouin scattering gain spectra in optical fibers[J]. Journal of lightwave technology, 2002, 20(8)：1425-1432.

[18]   PENG J, LU Y, ZHANG Z, et al. Distributed temperature and strain measurement based on Brillouin gain spectrum and Brillouin beat spectrum[J]. IEEE photonics technology letters, 2021, 33(21)：1217-1220.

[19]   ZASLAWSKI S, YANG Z, SOTO M A, et al. Impact of fitting and digital filtering on signal-to-noise ratio and Brillouin frequency shift uncertainty of BOTDA measurements[C]//2018 International Conference on Optical Fiber Sensors (OFS), September 24-28, 2018, Lausanne, Switzerland. Washington, DC：Optical Society of America, 2018：ThE27.

[20]   FARAHANI M A, CASTILLO-GUERRA E, COLPITTS B G. A detailed evaluation of the correlation-based method used for estimation of the Brillouin frequency shift in BOTDA sensors[J]. IEEE sensors journal, 2013, 13(12)：4589-4598.

[21]   HONG X B, ZHANG X Y, SUN X Z, et al. A fast method for Brillouin frequency shift estimation[J]. Sensors & actuators A physical, 2018, 284：6-11.